ChemComm

COMMUNICATION

View Article Online
View Journal | View Issue

Cite this: *Chem. Commun.*, 2016, 52, 13588

Received 25th July 2016,
Accepted 15th October 2016

DOI: 10.1039/c6cc06140k

www.rsc.org/chemcomm

N- and O-doped mesoporous carbons derived from rice grains: efficient metal-free electrocatalysts for hydrazine oxidation†

Katherine Koh,‡[a] Yuying Meng,‡[b] Xiaoxi Huang,[a] Xiaoxin Zou,[c] Manish Chhowalla[d] and Tewodros Asefa*[ae]

Nitrogen and oxygen co-doped mesoporous carbons that can serve as metal-free electrocatalysts are synthesized *via* a novel synthetic route using milled rice as a precursor and colloidal silica as a template. The materials efficiently electrocatalyze the hydrazine oxidation reaction with only a small onset potential, while giving a high peak current density and showing good long-term stability.

The rapid rise in energy demands worldwide and the environmental issues caused by burning fossil fuels around the globe have been pressing the scientific community to find solutions to these challenging problems. Fuel cells constitute one of the most promising solutions to these problems because they have the ability to convert chemical energy from various sustainable sources (such as hydrogen generated by solar-water electrolysis or ethanol derived from biomass hydrolysis) to electrical energy with reasonably high efficiency.[1] However, for fuel cells to work effectively, they require advanced, efficient and sustainable catalysts that promote the half reactions involved at the electrodes in them.[2,3] Among the many candidate catalysts developed so far for these purposes, heteroatom-doped carbon-based catalysts remain on the top of the list.[4,5] This is because these metal-free materials have an ability to electrocatalyze some of the most important yet difficult reactions used in various fuel cells as well as water electrolyzers, such as the oxygen reduction reaction (ORR),[6,7] the oxygen evolution reaction (OER),[8,9] the hydrogen evolution reaction (HER)[10,11] and the hydrazine oxidation reaction (HOR).[12]

It has been reported that these metal-free carbon catalysts can be synthesized from different synthetic precursors, for example, phenol[13] and various polymers.[7,12] However, using these precursors for making electrocatalysts not only is costly but also can generate toxic chemicals and is not in line with ongoing worldwide initiatives on the development of green and sustainable chemistry and materials. To address this issue, biomass, which is relatively inexpensive, abundant and renewable, is increasingly considered as precursor to make such metal-free catalysts. In fact, many previous studies in this area have shown that various carbon materials can be derived from biomaterials, such as peanut hulls, grass, soy milk, *etc.*, using various synthetic methods.[14–16] Moreover, some of these biomass-derived carbon materials have been reported to have comparable catalytic activity to those derived from synthetic precursors.[14,17] Hence, research efforts have continued to find other natural, renewable precursors as well as facile synthetic routes that can convert such raw materials or biomass wastes to efficient carbon-based catalysts.

One of the simplest synthetic approaches applied to synthesize carbon nanomaterials is a low temperature hydrothermal carbonization (HTC).[18,19] This synthetic method generally produces carbon materials possessing an amorphous structure and a high density of oxygen-based functional groups.[18,19] However, the method on its own is often ineffective in producing materials with high surface area—something that is highly required for many applications, including electrocatalysis.[18,19] To overcome this issue, we hypothesized that using sacrificial templates along with the carbon precursors during the HTC and pyrolysis processes can lead to carbon materials with highly porous structures, and thereby better electrocatalytic properties. While hard templates have been used to obtain porous structures and high surface areas in solid-state materials before,[20–22] they have never been combined with HTC and pyrolysis synthetic steps and applied together on biomass to produce porous carbon materials that are otherwise difficult to make.

To this end, herein we demonstrate that HTC and pyrolysis can be successfully applied on milled rice grains (Fig. S1 in the ESI†) in the presence of colloidal silica templates to generate rice-derived heteroatom-doped mesoporous carbons (called RDMCs). The resulting metal-free, nanoporous carbons are found to efficiently electrocatalyze HOR. Rice grains contain starch (90%, dry basis) and some proteins (7%),[23] and they can thus co-deliver the carbon

[a] *Department of Chemistry and Chemical Biology, Rutgers, The State University of New Jersey, Piscataway, New Jersey 08854, USA. E-mail: tasefa@rci.rutgers.edu*
[b] *School of Chemistry, Sun Yat-Sen University, Guangzhou 510275, P. R. China*
[c] *State Key Laboratory of Inorganic Synthesis and Preparative Chemistry, International Joint Research Laboratory of Nano-Micro Architecture Chemistry, College of Chemistry, Jilin University, Changchun 130012, P. R. China*
[d] *Department of Materials Science and Engineering, Rutgers, The State University of New Jersey, Piscataway, New Jersey 08854, USA*
[e] *Department of Chemical and Biochemical Engineering, Rutgers, The State University of New Jersey, Piscataway, New Jersey 08854, USA*

† Electronic supplementary information (ESI) available. See DOI: 10.1039/c6cc06140k

‡ K. Koh and Y. Meng contributed equally.

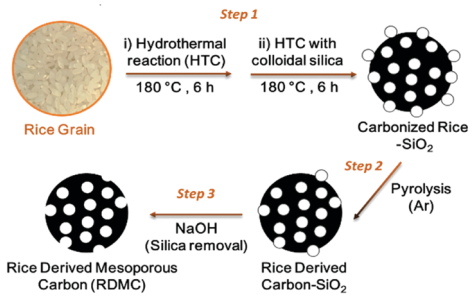

Scheme 1 Schematic procedure employed to synthesize the rice-derived mesoporous carbon (RDMC) materials.

atoms and heteroatoms needed to make heteroatom-doped carbon electrocatalysts during carbonization.[24] The synthesis of the materials is carried out through three major steps consisting of HTC (Step 1), high temperature pyrolysis (Step 2) and silica etching (Step 3), as illustrated in Scheme 1.

As described in detail in the ESI† section, the synthesis of the rice-derived mesoporous carbons (RDMCs) starts with a low temperature hydrothermal treatment of milled raw rice grains at 180 °C for 6 h. **Caution!** Autoclaves under hydrothermal conditions should be handled with extreme care and appropriate safety protocols. This is followed by an additional hydrothermal treatment of the materials in the presence of different amounts of colloidal silica templates at 180 °C for another 6 h. The carbonized rice-SiO_2 composite materials are then pyrolyzed at different high temperatures (600, 700, 800 or 900 °C). Finally, the silica templates in the carbonized products are removed using concentrated NaOH solution, in order to create nanopores in the carbon materials. By varying the pyrolysis temperatures as well as the amount of colloidal silica templates (0–2 g of colloidal silica per 1 g of rice grain), different RDMC materials, which are labeled RDMC-*T*-*x*, where *T* and *x* represent the final pyrolysis temperature and the amount of silica in g per 1 g of rice, respectively, are then obtained. Additionally, the following two control materials are synthesized. The first one, called RDC-HTC-1, is synthesized by applying only the two HTC treatment steps in the presence of 1 g of colloidal silica, followed by removal of silica templates (*i.e.*, with no additional pyrolysis step). The second one, denoted RDMC-800-Py-1, is synthesized by directly pyrolyzing a dried physical mixture of milled rice grains and colloidal silica (1 : 1 wt ratio) without the HTC treatment steps. The effects of these and other controlled synthetic conditions on the compositions, structures and electrocatalytic properties of the resulting materials toward the HOR are then investigated (see the ESI† for details).

The structures of RDMC-*T*-*x* and control materials are first examined by N_2 porosimetry (Fig. S2, ESI†). The results show that the surface area of the materials depends on both the amount of colloidal silica and the pyrolysis temperature used to synthesize them. As the amount of colloidal silica is increased, the Brunauer–Emmett–Teller (BET) surface area of the RDMC-800-*x* materials gradually increases. For example, the surface area of the materials increases from 14 $m^2\ g^{-1}$ for RDC-800-0 (which is synthesized without using colloidal silica templates) to 343 $m^2\ g^{-1}$ for RDMC-800-0.5 (which is synthesized using a moderate amount or 0.5 g of colloidal silica templates for 1 g of milled rice grains), and

Table 1 BET surface area, average BJH pore size, and pore volume of a series of RDMC-*T*-*x* materials

Entry	RDMC-*T*-*x*[a] *T*	*X*	BET surface area[b] ($m^2\ g^{-1}$)	Average pore size[b] (nm)	Pore volume[b] ($cm^3\ g^{-1}$)
1	800	0	14	N/A	N/A
2	800	0.5	343	15.1	0.9
3	800	1	366	18.5	1.0
4	800	2	520	11.1	1.0
5	600	1	686	12.4	1.1
6	700	1	557	15.5	1.2
7	900	1	343	13.8	0.8
8[c]	N/A	1	N/A	N/A	N/A
9[d]	800	1	164	11.0	0.1

[a] *T* represents the pyrolysis temperature and *x* represents the amount of colloidal silica (in g) per 1 g of milled rice grain. [b] Measured by N_2 porosimetry. [c] A control material, which is denoted as RDC-HTC-1. [d] A control material, labeled RDMC-800-Py-1.

then to 520 $m^2\ g^{-1}$ for RDMC-800-2 (which is synthesized using the highest amount of colloidal silica templates) (Table 1). The Barrett–Joyner–Halenda (BJH) pore size distribution reveals that the pore size of RDMC-800-*x* (where $x > 0.5$ g) is centered at *ca.* 12 nm, which is comparable to the size of colloidal silica used as templates for the synthesis of the materials. Note that RDC-800-0, which is synthesized without colloidal silica, is almost non-porous. The characterization results of the other relevant control materials are shown and compiled in Fig. S3–S5 and Tables S1 and S2 (ESI†).

On the other hand, as the pyrolysis temperature increases, the BET surface area of the carbon materials decreases. For example, the surface area is 686 $m^2\ g^{-1}$ for RDMC-600-1, but decreases to 343 $m^2\ g^{-1}$ for RDMC-900-1 (Table 1, entries 5–7). This trend is similar to other carbon materials synthesized from other precursors by pyrolysis and that are reported before.[25] The decrease in surface area at higher temperatures is likely the result of the higher degree of cross-linkages that the aliphatic and aromatic carbon atoms in the precursors undergo during carbonization at increasingly higher temperatures.[26]

Interestingly, there is no measurable porosity in RDC-HTC-1 (one of the control materials synthesized, entry 8 in Table 1). This indicates that the starch in the rice grains undergoes only hydrolysis, dehydration, and carbonization during the HTC step, and the silica nanoparticles cannot enter into the matrices of the resulting carbon material under the relatively low temperature employed during the HTC step. On the other hand, RDMC-800-Py-1 is nanoporous, and has a BET surface area of 164 $m^2\ g^{-1}$ (entry 9 in Table 1). Its surface area is, however, still lower than those of the materials synthesized by combining HTC and high temperature pyrolysis (*e.g.*, entry 3 in Table 1).

These results are further corroborated by TEM, which also shows that the structure of the materials changes from bulky, non-porous to nanoporous as colloidal silica is used in their synthesis (Fig. 3). For example, TEM images of the control material RDC-HTC-1 show non-porous structures whereas those of RDMC-800-Py-1 show porous structures (Fig. 1c and d). So, overall, the results above all indicate the importance of colloidal silica as templates and the HTC and high temperature pyrolysis steps to produce carbon materials with desirable high surface area nanoporous structures from rice grains.

The Raman spectra of RDMC-*T*-*x* materials display two broad peaks at *ca.* 1348 and 1586 cm^{-1}, corresponding to the characteristic

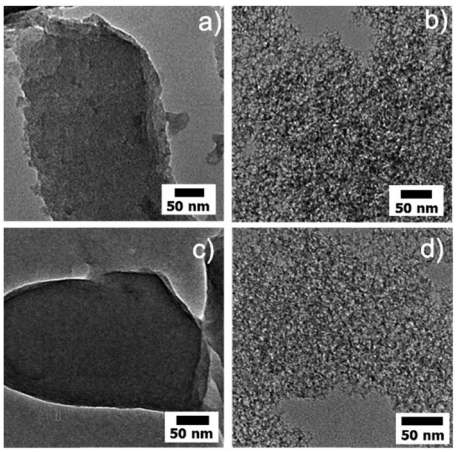

Fig. 1 TEM images of some representative RDMC and control materials: (a) RDC-800-0, (b) RDMC-800-1, (c) RDC-HTC-1, and (d) RDMC-800-Py-1. Additional images are provided in the ESI.†

D and G bands, respectively, of graphitic carbon materials (Fig. S6, ESI†).[27] The D band in such materials is generally associated with structural defects caused by heteroatom dopants, while the G band commonly represents the typical ordered domains of graphitic carbon materials.[7] Specifically, in the case of the RDMC materials, the D band most likely stems from the presence of N dopant atoms in the carbon structure, whereas the G band is due to the sp^2 carbon-related graphitic structure.[28] The value of the I_D/I_G ratio of RDMC-800-*x* materials, which represents the relative degree of disorder in the structure of carbon materials, is *ca.* 0.90 for all the materials (Fig. S6c and d, ESI†). This suggests that the relative ratio of defect-to-ordered domains in the materials is not greatly affected by the amount of colloidal silica templates used to make the materials. However, in the case of the series of PDMC-*T*-1 materials, the value of the I_D/I_G ratio increases significantly, from 0.74 to 0.94, when the pyrolysis temperature is increased from 600 to 900 °C.

The elemental composition of the materials is determined by X-ray photoelectron spectroscopy (XPS). In the XPS survey spectra of the RDMC materials (Fig. S7, ESI†), peaks corresponding primarily to C and O, and some to N, are seen. While the O atoms may have predominantly come from the starch, the N dopants have most likely come from the small amount of protein present in rice. The ratio of N/C in the RDMC-*T*-1 materials varies slightly, between 0.4 and 1.3%, with RDMC-700-1 showing the lowest amount of N (Fig. S8b, ESI†). There is some trend in O/C and N/C with respect to the amount of colloidal silica as well as the pyrolysis temperature used to make the materials. Although what may have caused the trends may need further investigations, some conclusions can still be drawn. It can be seen that, as the amount of colloidal silica increases up to a point, the porosity of the materials increases (Table 1), making the material easily lose N and O atoms, and have low N/C and O/C ratios. But, when the amount of colloidal silica increases further, despite the fact that the surface area of the material still increases, more oxygen from the colloidal silica also becomes available for the C atoms in the materials to escape with as CO_2, leaving behind relatively more N dopants. These two opposite processes are what may have made the materials with less or more colloidal silica than RDMC-800-0.5 to have higher amounts of N/C and O/C ratios. Furthermore, at higher temperature pyrolysis, some N and O are also likely to remain in the samples in the form of siliconoxynitride.

The chemical states of the nitrogen and carbon moieties in the materials are probed using high-resolution XPS (Fig. S9, ESI†). The peak corresponding to N1s is further deconvoluted into four different N dopant states, including pyridinic (398.7 eV), pyrrolic (400.3 eV), quaternary (401.2 eV) and pyridinic N^+–O^- (403.3 eV) species (Fig. S8c, ESI†).[29] In all the RDMC-*T*-1 materials, although the pyridinic moieties are conspicuous, their amount gradually decreases as the pyrolysis temperature is increased. On the other hand, the amount of quaternary nitrogen increases as the pyrolysis temperature is increased from 600 to 700 °C, but then remains almost unchanged after 700 °C. The deconvolution of the XPS peak for C1s for the series of RDMC-*T*-1 materials into three different states, corresponding to C=C–C (284.6 eV), C–O/C–N (286.1 eV) and C=O (287.5 eV), is also included (Fig. S8d, ESI†). The result shows that all RDMC-*T*-1 materials possess more C=C–C type groups than C–O/C–N and C=O type groups in their structures.

Cyclic voltammetry (CV) curves of HOR over the RDMC-*T*-*x* materials and the corresponding control samples from −0.6 V to 0.6 V (*vs.* SCE) at different scan rates for various hydrazine concentrations (Fig. 2 and Fig. S10–S18, ESI†) demonstrate that all the series of RDMC-800-*x* and RDMC-*T*-1 materials can effectively electrocatalyze HOR. Of all the materials, RDMC-800-1 shows the best catalytic activity with a relatively large negative onset potential of −0.34 V (*vs.* SCE) (or low overpotential), a large negative peak potential of −0.02 V (*vs.* SCE), and a high peak current density of 2.6 mA cm^{-2} in HOR of 50 mM hydrazine solution (Fig. 2a). The values obtained for RDMC-800-1 are also either comparable with or better than those obtained for other electrocatalysts, including 20 wt% Pt/C (Tables S3 and S4 and Fig. S16 in the ESI†).[12,30]

The current density produced during HOR over the RDMC materials increases linearly with the concentration of hydrazine (Fig. 2a and Fig. S10e and f, ESI†). Moreover, kinetic studies show

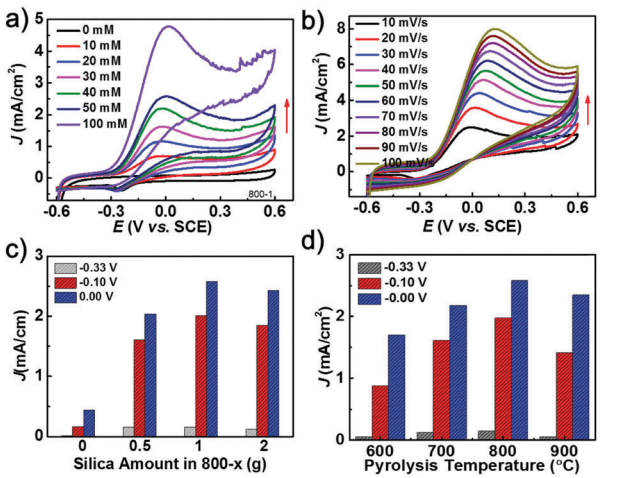

Fig. 2 Electrocatalytic activity of RDMC-800-1 for HOR: (a) in different concentrations of hydrazine at a scan rate of 10 mV s^{-1} and (b) at different scan rates in 50 mM of hydrazine. Comparison of current densities of HOR at three different potentials for the series of (c) RDMC-800-*x* and (d) RDMC-*T*-1 materials in 50 mM of hydrazine in 0.1 M PBS, pH 7.4, at a scan rate of 10 mV s^{-1}.

that increasing the electrochemical scan rates generates a more positive peak potential. The relationship between the peak current density and the square root of scan rate is linear, suggesting that the HOR over the materials involves a diffusion-controlled electrochemical process (Fig. 2b and Fig. S11e and f, ESI†). Additionally, no cathodic peak is observed during the whole reverse scans, indicating that the reaction is irreversible. This behavior is further corroborated by linear sweep voltammetry (LSV) using a rotating disk electrode (RDE) for RDMC-800-1 (Fig. S11, ESI†).

Next, the effects of surface area and pyrolysis temperature of the materials on the materials' electrocatalytic activities were probed. As can be seen in Fig. 3, the materials synthesized using relatively more colloidal silica templates show better electrocatalytic activity, with more negative onset and/or peak potential and higher peak current density. For example, as the amount of colloidal silica (x) is increased from 0 to 0.5 and 1 g, the onset potential of the materials in HOR gets better or shifts to a more negative value (−0.16, −0.33, and −0.34, respectively). However, a further increase in the amount of silica, or concomitantly surface area, does not appear to improve the catalytic activity of the materials any more; for example, when x is increased from 1 to 2, the onset potential remains almost unchanged while the current density, in fact, slightly decreases (Fig. 2c and d and Fig. S17, ESI†).

On the other hand, when the pyrolysis temperature is increased from 600 to 800 °C, the materials' electrocatalytic activity gradually improves (Fig. 3); however, when the pyrolysis temperature is increased from 800 to 900 °C, the materials' electrocatalytic activity decreases. The former may have to do with the increase in the dopant-related defect sites (Fig. S6b, ESI†) and the higher density of certain heteroatom species favorable for the electrocatalytic reaction in the material, such as quaternary N-species (Fig. S8, ESI†).[7,28] This is also why, we believe, RDMC-800-1 shows the best catalytic activity among the RDMC-T-1 materials we have investigated (Fig. 2d). Notably also, the control materials, RDC-HTC-1 and RDMC-800-Py-1, show poor catalytic activity; this indirectly suggests that both HTC and high temperature pyrolysis are essential to make the highly active catalytic materials obtained here (Fig. S12, ESI†).

Next, the stability of the materials during electrocatalysis is evaluated (Fig. S17, ESI†). After 500 cycles, the current densities during HOR over RDMC-800-1 remain as much as the initial values (Fig. S17a, ESI†), indicating the stability of the material during catalysis. This is confirmed by chronoamperometry or i–t measurements (Fig. S17b, ESI†).

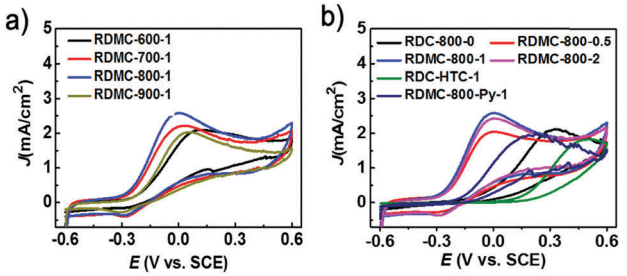

Fig. 3 CVs of HOR of 50 mM hydrazine at pH 7.4 in 0.1 M PBS with a scan rate of 10 mV s^{-1} over the series of (a) RDMC-T-1 and (b) RDMC-800-x materials and their corresponding control materials.

In conclusion, nitrogen and oxygen co-doped mesoporous carbons have been synthesized from milled rice grains by combining hydrothermal carbonization with high temperature pyrolysis in the presence of colloidal silica templates. The as-obtained RDMCs have been demonstrated to serve as metal-free electrocatalysts for HOR. Their electrocatalytic performances have been found to depend on the synthesis parameters, particularly the pyrolysis temperature and the amount of colloidal silica templates used to make them.

This work was financially supported by the US NSF (DMR-1508611).

Notes and references

1 B. C. H. Steele and A. Heinzel, *Nature*, 2001, **414**, 345.
2 L. Wei, H. E. Karahan, S. Zhai, Y. Yuan, Q. Qiana, K. Goh, A. K. Ng and Y. Chen, *J. Energy Chem.*, 2016, **25**, 191.
3 W. Zhou, J. Zhou, Y. Zhou, J. Lu, K. Zhou, L. Yang, Z. Tang, L. Li and S. Chen, *Chem. Mater.*, 2015, **27**, 2026.
4 (*a*) Y. Liang, Y. Li, H. Wang, J. Zhou, J. Wang, T. Regier and H. Dai, *Nat. Mater.*, 2011, **10**, 780; (*b*) D. Yu, L. Wei, W. Jiang, H. Wang, B. Sun, Q. Zhang, K. Goh, R. Sia and Y. Chen, *Nanoscale*, 2013, **5**, 3457.
5 X. Zou, X. Huang, A. Goswami, R. Silva, B. R. Sathe, E. Mikmekov and T. Asefa, *Angew. Chem., Int. Ed.*, 2014, **126**, 4461.
6 K. Gong, F. Du, Z. Xia, M. Durstock and L. Dai, *Science*, 2009, **323**, 760.
7 R. Silva, D. Voiry, M. Chhowalla and T. Asefa, *J. Am. Chem. Soc.*, 2013, **135**, 7823.
8 K. Sakaushi, T.-P. Fellinger and M. Antonietti, *ChemSusChem*, 2015, **8**, 1156.
9 X. Lu, W.-L. Yim, B. H. R. Suryanto and C. Zhao, *J. Am. Chem. Soc.*, 2015, **137**, 2901.
10 Y. Zheng, Y. Jiao, M. Jaroniec and S. Z. Qiao, *Angew. Chem., Int. Ed.*, 2015, **54**, 52.
11 J. Deng, P. Ren, D. Deng and X. Bao, *Angew. Chem., Int. Ed.*, 2015, **54**, 2100.
12 Y. Meng, X. Zou, X. Huang, A. Goswami, Z. Liu and T. Asefa, *Adv. Mater.*, 2014, **26**, 6510.
13 D. S. Yang, D. Bhattacharjya, S. Inamdar, J. Park and J. S. Yu, *J. Am. Chem. Soc.*, 2012, **134**, 16127.
14 (*a*) L. Wei, H. E. Karahan, K. Goh, W. Jiang, D. Yu, Ö. Birer, R. Jiang and Y. Chen, *J. Mater. Chem. A*, 2015, **3**, 7210; (*b*) L. Wei, D. Yu, H. E. Karahan, Ö. Birer, K. Goh, Y. Yuan, W. Jiang, W. Liang and Y. Chen, *Catal. Today*, 2015, **249**, 228.
15 B. S. Girgis, S. S. Yunis and A. M. Soliman, *Mater. Lett.*, 2002, **57**, 164.
16 S. Liu, J. Tian, L. Wang, Y. Zhang, X. Qin, Y. Luo, A. M. Asiri, A. O. AlYoubi and X. Sun, *Adv. Mater.*, 2012, **24**, 2037.
17 Y. Zhai, C. Zhu, E. Wang and S. Dong, *Nanoscale*, 2014, **6**, 2964.
18 S.-H. Yu, X. Cui, L. Li, K. Li, B. Yu, M. Antonietti and H. Cölfen, *Adv. Mater.*, 2004, **16**, 1636.
19 Y. Yang, J. Cui, M. Zheng, C. Hu, S. Tan, Y. Xiao, Q. Yang and Y. Liu, *Chem. Commun.*, 2012, **48**, 380.
20 L. Wei, M. Sevilla, A. B. Fuertes, R. Mokaya and G. Yushin, *Adv. Energy Mater.*, 2011, **1**, 356.
21 C. Liang, Z. Li and S. Dai, *Angew. Chem., Int. Ed.*, 2008, **47**, 3696.
22 R. Liu, D. Wu, X. Feng and K. Müllen, *Angew. Chem., Int. Ed.*, 2010, **122**, 2619.
23 B. O. Juliano, *Chemical Aspects of Rice Grain Quality*, International Rice Research Institute, Philippines, 1st edn, 1979.
24 Y. Zheng, Y. Jiao, L. Ge, M. Jaroniec and S. Z. Qiao, *Angew. Chem., Int. Ed.*, 2013, **125**, 3192.
25 Y. Chen, H. Yang, X. Wang, S. Zhang and H. Chen, *Bioresour. Technol.*, 2012, **107**, 411.
26 K. Ishimaru, T. Hata, P. Bronsveld, D. Meier and Y. Mamura, *J. Mater. Sci.*, 2007, **42**, 122.
27 W. Qian, R. Hao, Y. Hou, Y. Tian, C. Shen, H. Gao and X. Liang, *Nano Res.*, 2009, **2**, 706.
28 R. Silva, J. Al-Sharab and T. Asefa, *Angew. Chem., Int. Ed.*, 2012, **51**, 7171.
29 P. H. Matter, L. Zhang and U. S. Ozkan, *J. Catal.*, 2006, **239**, 83.
30 X. Huang, X. Zou, Y. Meng, E. Mikmeková, H. Chen, D. Voiry, A. Goswami, M. Chhowalla and T. Asefa, *ACS Appl. Mater. Interfaces*, 2015, **7**, 1978.